Heterogeneous Catalysis Hot Paper

Zitierweise: *Angew. Chem. Int. Ed.* **2020**, *59*, 20973 – 20979
Internationale Ausgabe: doi.org/10.1002/anie.202005616
Deutsche Ausgabe: doi.org/10.1002/ange.202005616

Scaling Platinum-Catalyzed Hydrogen Dissociation on Corrugated Surfaces

*Sabine V. Auras, Richard van Lent, Dima Bashlakov[+], Jessika M. Piñeiros Bastidas[+], Tycho Roorda[+], Rick Spierenburg[+] und Ludo B. F. Juurlink**

Abstract: *We determine absolute reactivities for dissociation at low coordinated Pt sites. Two curved Pt(111) single-crystal surfaces allow us to probe either straight or highly kinked step edges with molecules impinging at a low impact energy. A model extracts the average reactivity of inner and outer kink atoms, which is compared to the reactivity of straight A- and B-type steps. Local surface coordination numbers do not adequately capture reactivity trends for H_2 dissociation. We utilize the increase of reactivity with step density to determine the area over which a step causes increased dissociation. This step-type specific reactive area extends beyond the step edge onto the (111) terrace. It defines the reaction cross-section for H_2 dissociation at the step, bypassing assumptions about contributions of individual types of surface atoms. Our results stress the non-local nature of H_2 interaction with a surface and provide insight into reactivity differences for nearly identical step sites.*

Introduction

For gas-phase reactions involving the smallest of molecules, H_2, accurate theoretical descriptions are nowadays available and match experimental results.[1] However, the same remains challenging for gas-surface reactions.[2] The involvement of many atoms in the surface complicates the description of energy dissipation mechanisms, amongst others. The chemically accurate prediction of reactivity for the highly activated H_2 dissociation on Cu(111), using quantum dynamics calculations and density functional theory (DFT)-based potentials, is exceptional.[3] In other cases, simplifications in the description of the system are needed to lower the computational effort, and show continuing advancements. A relevant example is the successful application of quasi-classical trajectory calculations for the more reactive H_2 dissociation on Pt(111).[4]

Reactions on high Miller index surfaces, such as regularly stepped surfaces, have often been claimed to be more relevant to real-world chemistry, for example, heterogeneous catalysis. Such vicinal surfaces contain lower coordinated surface atoms, for example, forming steps in terraces and kinks in steps, which resemble edges and corners on actual catalyst particles. Accurate calculations based on periodic potentials then require larger unit cells, hence much higher computational effort. The chemically accurate description of H_2 dissociation on Cu(211) is the state of the art.[5] The dissociation of a larger molecule, methane, can be described with chemical accuracy by ab initio molecular dynamics on select Pt surfaces, but the same approach does not describe reaction on a kinked surface to the same accuracy.[6–8]

The computational effort required to accurately describe the simplest dissociative event on well-defined surface structures highlights the challenges to constructing an accurate kinetic description for heterogeneous catalysis. Different methods are necessary to consider all surface sites available on a catalyst particle simultaneously. A recent addition to various approaches (see Ref. [9] for a thorough discussion) is the idea that one may generalize the reactivity dependence of surface sites on their coordination number.[10–12] Coordination numbers are commonly used in organic and inorganic chemistry. Consequently, it can seem intuitively logical to apply it to gas-surface interactions. To capture different surface geometries of nearly identical surface sites, a generalized coordination number, $\overline{CN}$, was introduced. It includes the coordination shell of all atoms neighboring the surface atom involved in the dissociation event. This concept was successfully applied in a study of bond energies of H- and O-containing adsorbates on Pt particles. The authors suggested it to be a predictive descriptor linking geometric arrangement of a surface to adsorption properties. As $\overline{CN}$ can simply be calculated by hand, it does not require electronic structure calculations.

Surface coordination approaches shift the focus in our chemical thinking about bond breaking from the impinging molecule probing a surface potential, towards the local properties of the site of reaction. While for many systems, this may be acceptable and appropriate, we wonder whether it applies to the dissociative adsorption of H_2. First, the two types of straight step edges occurring on (111) facets of *fcc*

[*] S. V. Auras, Dr. R. van Lent, J. M. Piñeiros Bastidas,[+] T. Roorda,[+] R. Spierenburg,[+] Assoc. Prof. L. B. F. Juurlink
Leiden Institute of Chemistry, Leiden University
P.O. Box 9502, 2300 RA Leiden (The Netherlands)
E-Mail: l.juurlink@chem.leidenuniv.nl

Dr. D. Bashlakov[+]
ILTPE, National Academy of Sciences of Ukraine
47 Nauky Ave., Kharkiv 61103 (Ukraine)

[+] These authors contributed equally to this work.

Supporting information and the ORCID identification number(s) for the author(s) of this article can be found under: https://doi.org/10.1002/anie.202005616.

metals, for example, Pt or Ni, provide the same coordination numbers at the upper step edge, but are found to be chemically unique in desorption of H_2 (see, for example, Refs. [13,14]). Second, the quantum dynamical nature of the molecule may allow it to probe the surrounding potential energy surface (PES) bypassing the highly localized nature of the collision as imposed by a coordination number approach. Dynamical calculations for H_2 interaction with Pt(211) by Baerends and co-workers suggested this: At low collisional energy, dissociation predominantly occurs via a dynamical chemisorbed molecular state that dissociates barrier-free at the upper edge of a step even though its center of mass impinged at the inner cusp.[15,16]

Recent advances in the use of curved surfaces of single crystal samples allow us to critically evaluate the relation between dissociative reaction dynamics and the structure of the surface.[17,18] Here, we use two Pt curved single crystals exposing surface atoms with various coordination numbers and local surface geometries to determine whether the dissociation of molecular hydrogen on platinum follows trends predicted by coordination number approaches. We experimentally determine the dissociation probability for molecular hydrogen along the curvatures and relate the absolute reactivity to the local structure of steps and kinks.

Results and Discussion

We impinge D_2 from a molecular beam onto the curved surfaces of two Pt crystals to determine the initial sticking probability (S_0). As D_2 chemisorbs dissociatively at the applied surface temperature of 155 K, sticking probabilities correspond to dissociation probabilities. The schematics of the curved samples and the relative size of the beam impinging on the surface with a rectangular profile are shown in Figure 1 a. Both Pt crystals contain the (111) surface at their apex and curve 15.5° to either side. The macroscopic curvature of the Pt crystals results from the introduction of a single step type with smoothly increasing density when moving toward the crystal's edges. The supersonic beam always impinges normal to the (111) terraces.

The two curved surfaces contain three different step structures. On the crystal with a $[1\bar{1}0]$ rotational axis, (001)-oriented (or A-type) steps and (110)-oriented (or B-type) steps occur separately on the two sides of the apex. The second crystal has its rotational axis oriented along $[11\bar{2}]$, exhibiting facets of the (201) and (021) planes, forming kinked steps. As their direction lies halfway in between A- and B-type steps, the kinked steps consist of short, alternating sections of A- and B-steps connected by inner and outer kinks. The kinked steps give rise to chiral stepped surfaces with opposite handedness on the two sides of the crystal. The chirality is not expected to impact reactivity for the achiral H_2. We therefore refer to the kinked steps on either side of the crystal as {210}-oriented steps (we use Miller indices {hkl} to indicate the set of equivalent surfaces). A- and B-type and kinked step structures in their ideal form are shown in Figure 1 b. Note that we show the fully kinked step facets for the {210} case.

Figure 1 c plots S_0 of D_2 as a function of step density for an average kinetic energy of 9.3 meV. The hatched area indicates where the crystal surface becomes more narrow than the beam due to the shape of our samples. The data are averages of multiple measurements on the same location of a curved surface. Error bars reflect one standard deviation of the average value. For the crystal with kinked steps, data from both sides of the crystal are included, but do not vary appreciably. At the (111) apices of the two crystals we measure an $S_0^{(111)}$ of 0.011 ± 0.018 and 0.032 ± 0.013 respectively, in good agreement with previous studies on flat Pt(111) surfaces for similar collision energies.[19–21] To the sides of the crystals, S_0 increases linearly with step density for all step types over the range where the molecular beam fits onto the crystal surface. Scalability of the reactivity of stepped surfaces

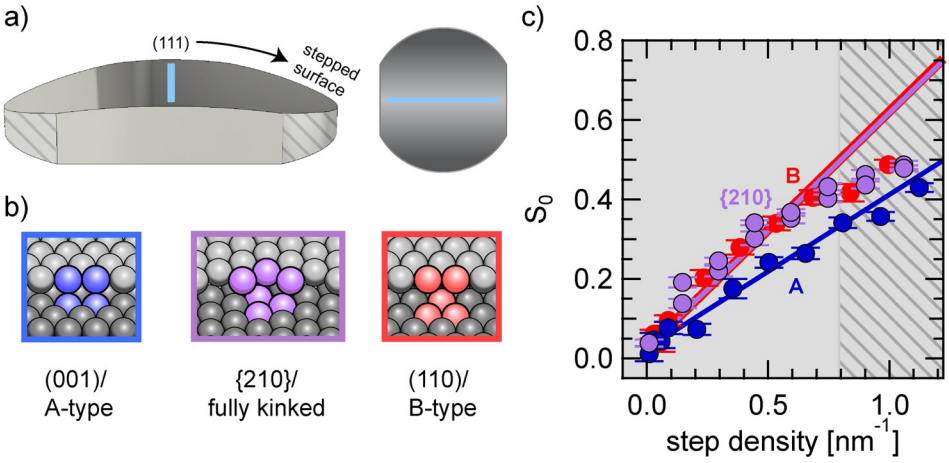

Figure 1. a) Representations of the side and top view of the curved crystals and the hydrogen beam impinging onto a 0.126 nm wide section of the surface (light blue line). At the sides, the width of the crystal narrows as indicated by the hashed areas. b) Structures of the three step types found on the two curved crystals. For the kinked step edges, we display the fully-kinked form. c) Sticking probabilities S_0 of D_2 as a function of step density for the two different Pt surfaces at $E_{kin} = 9.3$ meV and $T_{surface} = 155$ K. Colored markers indicate sticking on (111) surfaces with A-type (blue), B-type (red), and highly kinked steps (purple). The hashed part of the plot indicates the area where the crystals are narrower than the impinging molecular beam. Blue, red, and purple lines are linear fits to the data.

was previously suggested for A-type steps.[15] Here S_0 can be described for all stepped surfaces as [Eq. (1)]:

$$S_0(SD) = S_0^{(111)} + \Sigma_0 \cdot SD \quad (1)$$

where SD is the step density and Σ_0 the rate of increasing S_0 with step density (that is, the slope). Σ_0 quantifies the reactivity of the step type at the incident energy used here (see the Supporting Information for a detailed discussion on the relation of Σ_0 and the sticking probabilities at steps S_0^{step}). We apply linear fits to the data with appropriate weighting to compare Σ_0 for these step types. Here, we exclude data from the hatched area and fix $S_0^{(111)}$ at the average of the two values determined for (111) on the two separate single crystals, that is, 0.025. For the crystal with kinked steps, we use data of both sides in a single fit. The resulting linear fits are displayed with colors matching the data. The extracted values for Σ_0 are listed in Table 1. While Σ_0 for B-type and {210} steps are almost equal, that is, about 0.6 nm, the A-type steps show a significantly smaller increase in reactivity with step density, that is, about 0.4 nm.

While it is sometimes assumed that kinks would be more reactive than straight step edges, which in turn would be more reactive than flat terraces, our data at first glance does not represent this trend. However, the Σ_0 value we obtain for the {210} steps here does not necessarily reflect dissociation at ideal fully-kinked step. The kinked steps present on the surface may differ from the representation provided in Figure 1 a. The surface can maintain its overall crystallographic orientation while breaking the fully kinked step into larger segments (or microfacets) of A- and B-type steps, as observed for kinked Ag steps.[22] Figure 2 a illustrates two slightly longer segments. The number of kink sites is reduced from the fully kinked edge (section a) by introducing either 1 atom (section b) or 2 atoms (section c) in between kinks. Increasing the segment lengths decreases the kink density. To better understand the observed reactivity trend, we hereinafter determine the structural composition of the {210} steps using STM and apply a model that deconvolutes the contribution of inner and outer kinks.

Typical STM images with step arrays ranging from a step density of 0.086 nm^{-1} to 0.909 nm^{-1} are shown in Figure 2 b–e.

Tabelle 1: Step types and their coordination (*CN*) and generalized coordination numbers ($\overline{CN}$) at the upper step edge.[a]

Step type	Coordination (upper edge)		Σ_0 [nm]	*a* [nm]	σ_0 [nm^2]
	CN	$\overline{CN}$			
A/ (001)	7	5.50	0.387	0.277	0.107
B/ (110)	7	5.50	0.597	0.277	0.165
real kinked/ {210}			0.593	0.48	0.285
fully kinked (max)	8*/ 6^+	6.17*/ 4.83^+	0.726	0.48	0.348

[a] For the kinked step coordination numbers for the inner (*) and outer (+) kinks are listed. Rates of increasing sticking with step density (Σ_0) are determined by linear fits of the S_0 data in Figure 1 for the first three rows. The value of Σ_0 in the bottom row is derived from Equation (4). Multiplying Σ_0 with unit cells widths of the stepped surfaces (*a*) gives the resulting reaction cross sections (σ_0) of the three types of steps. Note that the unit cell width is considerably larger for the kinked step.

We determine the outline of the step (shown as colored lines) by taking line profiles and determining the local height gradient. We then determined the length of all segments separated by inner and outer kinks along the step edge. This process is repeated for multiple steps in the image. Histograms on the right side of Figure 2 are normalized to represent the average percentage of segments with a length of one, two, three atoms, and so on. They are shown separately for both A- (blue) and B-type (red) microfacets. Each consecutive bin in the histograms represents a microfacet of one additional atom length. The lettering of the bins corresponds to the sections indicated in Figure 2 a.

The histograms in Figure 2 show that approximately half of the segments forming {210} steps on Pt are ideal, that is, they are fully-kinked. Roughly 40 to 60 % of the sections are in bin a. The remaining sections are longer, but very rarely do we observe segments of more than 5 atoms. All histograms show a similar smooth decrease in observed frequency with microfacet length from bin b onward. The distributions are independent of the average terrace width over the probed range of 43.0 atom rows in Figure 2 b to 4.1 atom rows in Figure 2 e. This confirms that the linear increase in S_0 observed in Figure 1 does not result from changes in the structure of {210} steps, but is exclusively caused by increasing step density. Furthermore, the distributions of A- and B-type facets are similar and suggest no preference for longer or shorter segments of one microfacet type despite varying line free energies of A- and B-type steps.[23]

From the distributions in Figure 2 and the atomic compositions for microfacets with varying lengths (Supporting Information, Table S2), we calculate the average number of kink (N_K), A-type (N_A), and B-type (N_B) atoms in an edge consisting of 100 segments in {001} orientation and 100 segments in {110} orientation. The total number of atoms in these 200 segments is given in Equation (2):

$$N = N_A + N_B + N_K \quad (2)$$

The fractional occurrence of kinks along a step is given by N_K/N. It consistently lies between 0.4 and 0.5 in all STM images (see the Supporting Information). Assuming that additional atoms in microfacets exhibit the reactivity of the A- (blue) or B-type steps (red), we now define the reactivity of {210} steps ($\Sigma_0^{\{210\}}$) as a weighted average of reactivities of kink atoms, A-type atoms (Σ_0^A), and B-type atoms (Σ_0^B) in all segments and set it equal to the experimentally determined value from Table 1 [Eq. (3)]:

$$\Sigma_0^{\{210\}} = \frac{N_K\Sigma_0^K + N_A\Sigma_0^A + N_B\Sigma_0^B}{N} = 0.593\text{nm} \quad (3)$$

We solve for Σ_0^K using the data from individual STM images and the already known values for Σ_0^A and Σ_0^B. Table S3 in the Supporting Information lists the results. The average value of Σ_0^K is 0.726 nm. As our model enforces lower reactivities for all A- and B-type atoms in longer segments of kinked steps, it is the upper limit for the average reactivity of inner and outer kinks [Eq. (4)]:

$$\Sigma_0^K = (\Sigma_0^{K_{in}} + \Sigma_0^{K_{out}})/2 = 0.726\text{nm} \quad (4)$$

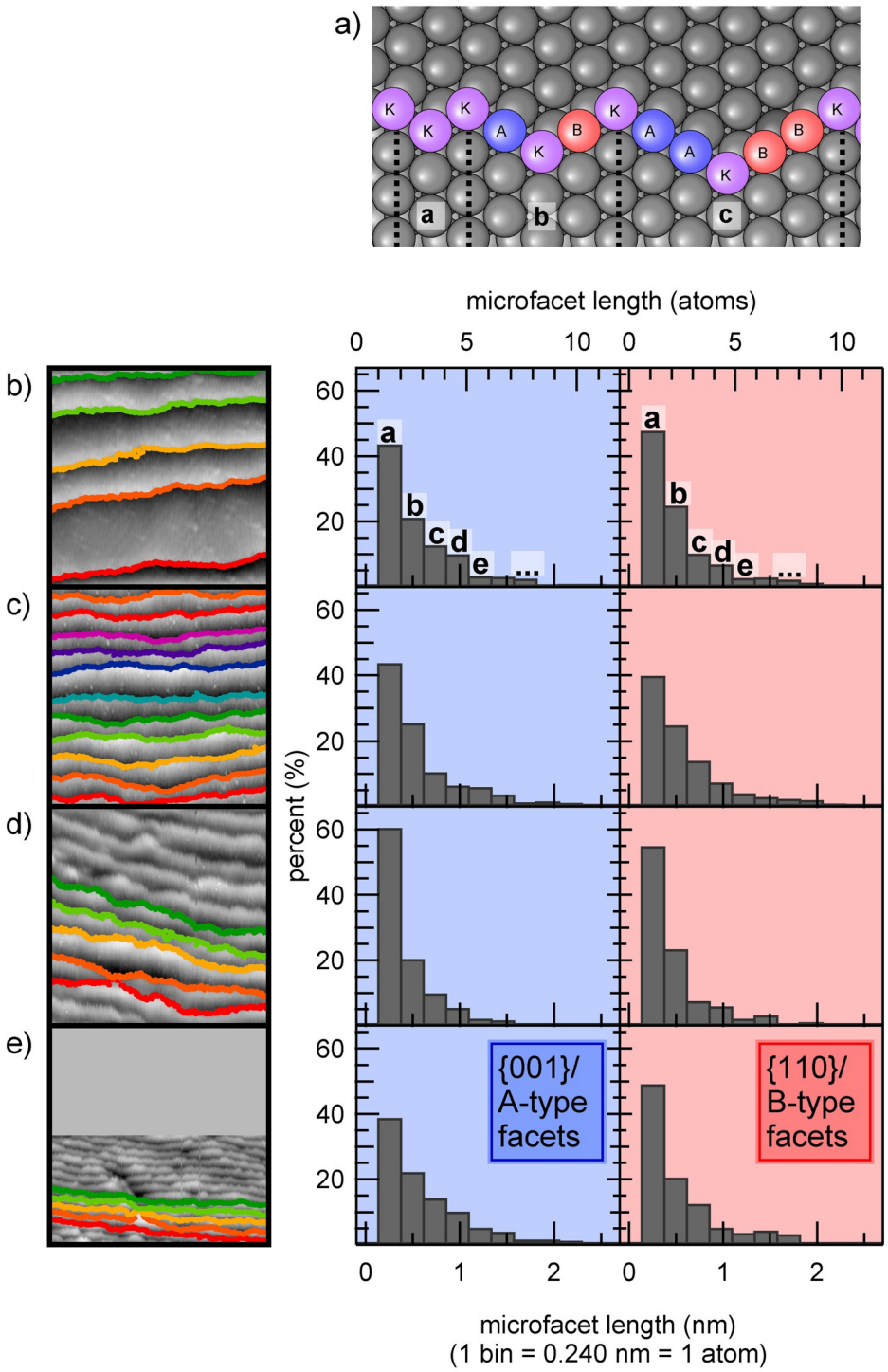

Figure 2. a) Kinked step edge with different widths of its {001}- and {110}-oriented segments. In a, segments are only one atom wide. Each atom is either at an inner or an outer kink site (purple). In b, two atom wide segments are formed. Half of the atoms are still kink sites, but in each orientation one atom is not directly a kink atom. These could be considered part of a short A-type (blue) or B-type (red) step segment. In c, three atom wide segments are formed. Only one third of all atoms in the step edge are direct kink atoms. b)–e) Left: STM images from various positions on the curved crystal. Colored lines indicate step edge contours as found by our analysis procedure. b) image size: 53×53 nm; mean terrace width: 11.6 nm/ 43.0 atoms. c) image size: 50×50 nm; mean terrace width: 4.6 nm/ 17.0 atoms. d) image size: 17×17 nm; mean terrace width: 1.7 nm/ 6.3 atoms. e) image size: 15×30 nm; mean terrace width: 1.1 nm/ 4.1 atoms. b)–e) Right: Corresponding histograms of facet lengths along the step edge. Blue panel: facets oriented in {001}-direction. Red panel: facets oriented in {110} direction. The first column of each histogram contains 1 atom wide microfacets, the second column 2 atom wide microfacets, and so on.

This maximum reactivity for the ideal or fully kinked step edge is shown in Table 1 and used to define the upper limit of average kink reactivity in Figure 3 (light purple line). This graph also shows a lower limit. It is derived from assuming that the facets along the kinked step edge act as type A and B steps with no additional reactivity of kinks. This situation is identical to a {210} step edge that is fully reconstructed, containing large stretches of both the A-type and B-type steps (with a kink density comparable to that typically occurring in A- or B-type steps). Its slope is given by [Eq. (5)]:

$$\frac{1}{2}\cdot(\Sigma_0^A+\Sigma_0^B)\cdot 1.16 = 0.570\text{nm} \quad (5)$$

The factor 1.16 accounts for the increased length of the step compared to a straight line connecting the first and last atom of a {210} step. The range of Σ_0^K as defined by these two extremes is indicated as the purple shaded area (in between the lines representing no kinks and only kinks) in Figure 3b.

The reactivity of the kink sites may hence indeed exceed that of straight step edges, as expected by the reduced number of nearest numbers at the outer kinks. The lower reactivity of the A-type step, however, remains unexpected from a coordination number viewpoint. As listed in Table 1, the number of nearest neighbors (coordination number *CN*) is identical for atoms forming the A- and B-type steps, that is, $CN=7$. On fully kinked steps, *CN* varies for the inner and outer kinks, being 8 and 6 respectively. Depending on their relative contribution to reactivity, their weighted average may coincide or deviate from straight steps. Based on *CN* alone, however, it cannot coincide with the B-type and deviate from the A-type. In fact, the difference in reactivity for the A and B-types already disagrees with *CN*. The inconsistency is also not resolved when considering coordination of atoms in the lower plane of the step, as discussed in the Supporting Information.

As *CN* fails to predict the reactivity trend, we verify whether the generalized coordination number, $\overline{CN}$, captures it. $\overline{CN}$ averages over all *CN* values belonging to the nearest neighbors of an atom, hence capturing more of the surroundings of the surface atom involved in the chemical event.[10] Table 1 presents values for $\overline{CN}$. Again, reactivity is not represented properly. On the basis of upper edge atoms alone, the three edge types would be identical in reactivity if the average of inner and outer kinks is used. If one considers only the outer kinks, then kinked edges should have been considerably more reactive than both A- and B-type edges and the latter should have been identical in reactivity. Although our analysis suggests that fully kinked steps are likely more reactive than B-type steps, approaches considering reactivity of each atom site individually continue to fail representing the clear variations in reactivity of all three step types.

Abandoning atomistic approaches, where we consider the local reactivity of each surface atom, we swing our viewpoint back to a non-local nature of the interaction of D_2 with the stepped surface as suggested by earlier dynamical calculations. Earlier experimental and theoretical dynamics studies using vicinal Pt surfaces suggest that three dissociation mechanisms occur in parallel.[15,24–26] First, dissociation at the upper edge is direct and non-activated. Second, molecules impinging into the bottom cusp of the step may be dynamically trapped and react by following shallow potential wells leading toward the upper edge. Third, molecules impinging on (111) terrace sites encounter modest activation barriers. While the value of $S_0^{(111)}$ was shown to be small at low collision energies, a linear combination of three contributions explains the observed dependence on step density shown in Figures 1 and 3. The slope (Σ_0) then gives the average length (measured normal to the edge) over which the step contributes to reactivity. It represents the cross section for the dissociation mechanisms related to steps, but reduced to a single spatial dimension.

Consequently, multiplying this length by the unit cell width (a) yields the initial reaction cross section (σ_0) [Eq. (6)]:

$$\sigma_0 = \Sigma_0 \times a \quad (6)$$

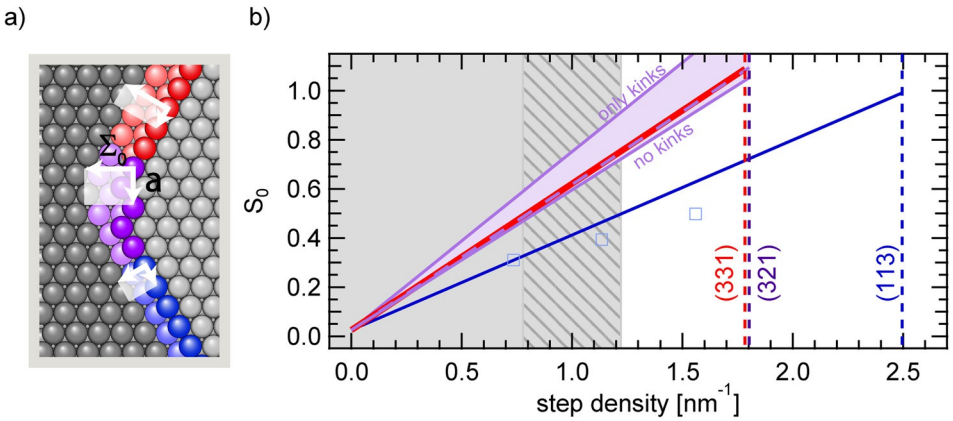

Figure 3. a) Relative positions of A-type, B-type, and kinked steps on a (111) terrace. The absolute reaction cross-section of each type as listed in Table 1 is indicated by white rectangles. Top to bottom: B-type, {210} (real), A-type. b) Extended fits (blue, red, dashed purple lines) of the S_0 data from Figure 1. The shaded purple area indicated the expected sticking behavior of the kinked step in the limits of only kinks and large faceting with minimal kinks. Blue squares: data from Ref. [24] for stepped surfaces, (extrapolated to $E_{kin}=9.3$ meV, S_0 measured under an incident angle along surface normal). Dashed vertical lines: Step densities of (331) (red), (321) (purple), and (113) (blue).

The values we obtain for σ_0 per step type are included in Table 1. They are also illustrated as white areas at the different edge types in Figure 3a. They may be compared to the area of molecular wells and the holes leading to non-activated dissociation in a PES. For the A-type, we have shown previously that it corresponds well to the reactive area of the PES calculated for H_2/Pt(211).[17] Our data suggests sizes of these areas for the B-type step and the corrugated {210}-type step. Both extend further onto the lower terrace than for the A-type step. Note that the larger σ_0 value for the {210} steps in Table 1 is partially caused by a larger unit cell width *a*.

The step-type dependence of σ_0 for D_2 colliding at less than than 10 meV in kinetic energy indicates that the distance over which steps may induce dynamical trapping and/or barrier-free dissociation critically depends on the local atomic arrangement in the step. For the A-type step, dissociation on the upper edge was found to be entirely barrier-free.[15] It is likely that the upper edges for the B-type and kinked edges also have these holes in the potential. The difference we find for the various edges must then result from the capability to trap molecular hydrogen in the cusp of the step. For A-type steps, the molecular adsorption wells that cause trapping with subsequent dissociation are then the smallest. B-type steps trap and dissociate molecular hydrogen over a longer distance. This may be caused by the relative shifts of the upper and second layers of Pt atoms at these steps. For the B-type step, the lateral shift is 2/3 of the distance between atom rows parallel to the edge, whereas it is only 1/3 for the A-type. Kinks appear to cause an even larger disturbance to the local potential with deeper and/or wider wells.

Finally, in Figure 3b, we extrapolate the fits with slope Σ_0 to predict reactivity beyond the range offered by our curved crystals to the highest possible step density for each step type, as indicated by the dashed lines. Our predictions for A-type steps agree reasonably well with the only published data obtained for surfaces with very short terraces, added as blue squares in Figure 3b.[24]

Surfaces featuring short terraces of only a few atom rows, such as those that we approach with the extrapolation in Figure 3b are particularly interesting to heterogeneous catalysis, as they are featured on the surface of real nanoparticles.[27] Only the equilibrium shape of very small metal particles of < 1 nm size one would expect to find sharp edges that do not feature a cusp to the adjacent terrace. There, the reactivities may vary from the ones derived here, due to the absence of dynamical trapping at the cusp. An impinging H_2 wavepacket would thus experience a smaller cross-section with such an edge than the ones derived here. For larger Pt nanoparticles, as well as regularly stepped Pt surfaces, we expect the chemical step size Σ_0 to be a reliable descriptor of reactivity towards D_2 dissociation.

Conclusion

Our examination of Pt-catalyzed hydrogen dissociation on surfaces with close-packed and highly-kinked steps yields reactivities for different surface structural features. STM analysis of kinked steps allows us to extract an average reactivity for inner and outer kinks. Results show that kinks likely aid dissociation more than atoms in straight steps. However, the measured reactivity difference for the two close-packed step types is not adequately captured by models that rely on counting (nearest) neighbors of various types of surface atoms. We believe that the origin of the discrepancy is the dynamical nature of the interaction. For a light-weight molecule interacting at low collision energy with a surface that is characterized by (at most) modest barriers to dissociation, molecular wells close to the dissociation site increase the dissociation probability. We therefore consider the interaction in terms of a cross section, σ_0. It reflects the physical area near the step where impingement leads to trapping and dissociation as found in earlier theoretical dynamics studies. The average length of this area, Σ_0, measured normal to the step, is derived directly from the experimentally determined dependence of reactivity on step density. We believe that the reactivities determined here, including the rule of thumb resulting from extrapolating experimental data to the smallest unit cells, provide a useful tool for modeling dissociation on vicinal surfaces with potentially large unit cells. Furthermore, they allow careful prediction of reactivities on industrially relevant catalyst sites by bridging the whole range of stepped Pt surfaces.

Acknowledgements

This work was financially supported by the Leiden Institute of Chemistry and the Netherlands Organisation for Scientific Research. The authors thank G.J. Kroes and H.F. Busnengo for helpful discussions.

Conflict of interest

The authors declare no conflict of interest.

Stichwörter: corrugated surfaces · heterogeneous catalysis · reaction cross-sections · reaction mechanisms · surface chemistry

[1] H. C. Schewe, Q. Ma, N. Vanhaecke, X. Wang, J. K. los, M. H. Alexander, S. Y. Van De Meerakker, G. Meijer, A. Van Der Avoird, P. J. Dagdigian, *J. Chem. Phys.* **2015**, *142*, 204310.
[2] G. J. Kroes, C. Díaz, *Chem. Soc. Rev.* **2016**, *45*, 3658 – 3700.
[3] C. Díaz, E. Pijper, R. A. Olsen, H. F. Busnengo, D. J. Auerbach, G. J. Kroes, *Science* **2009**, *326*, 832 – 834.
[4] E. Nour Ghassemi, M. Wijzenbroek, M. F. Somers, G. J. Kroes, *Chem. Phys. Lett.* **2017**, *683*, 329 – 335.
[5] E. W. Smeets, G. Füchsel, G. J. Kroes, *J. Phys. Chem. C* **2019**, *123*, 23049 – 23063.
[6] H. Chadwick, A. Gutiérrez-González, D. Migliorini, R. D. Beck, G. J. Kroes, *J. Phys. Chem. C* **2018**, *122*, 19652 – 19660.
[7] H. Chadwick, A. Gutiérrez-González, R. D. Beck, G. J. Kroes, *J. Chem. Phys.* **2019**, *150*, 124702.
[8] H. Chadwick, A. Gutiérrez-González, R. D. Beck, G. J. Kroes, *J. Phys. Chem. C* **2019**, *123*, 14530 – 14539.

[9] M. K. Sabbe, M. F. Reyniers, K. Reuter, *Catal. Sci. Technol.* **2012**, *2*, 2010 – 2024.
[10] F. Calle-Vallejo, J. I. Martínez, J. M. Garcá-Lastra, P. Sautet, D. Loffreda, *Angew. Chem. Int. Ed.* **2014**, *53*, 8316 – 8319; *Angew. Chem.* **2014**, *126*, 8456 – 8459.
[11] F. Calle-Vallejo, D. Loffreda, M. T. Koper, P. Sautet, *Nat. Chem.* **2015**, *7*, 403 – 410.
[12] F. Calle-Vallejo, J. Tymoczko, V. Colic, Q. H. Vu, M. D. Pohl, K. Morgenstern, D. Loffreda, P. Sautet, W. Schuhmann, A. S. Bandarenka, *Science* **2015**, *350*, 185 – 189.
[13] M. J. Van Der Niet, A. Den Dunnen, M. T. Koper, L. B. Juurlink, *Phys. Rev. Lett.* **2011**, *107*, 1 – 4.
[14] M. J. Kolb, A. L. Garden, C. Badan, J. A. Garrido Torres, E. Skúlason, L. B. Juurlink, H. Jónsson, M. T. Koper, *Phys. Chem. Chem. Phys.* **2019**, *21*, 17142 – 17151.
[15] D. A. McCormack, R. A. Olsen, E. J. Baerends, *J. Chem. Phys.* **2005**, *122*, 194708.
[16] R. A. Olsen, D. A. McCormack, M. Luppi, E. J. Baerends, *J. Chem. Phys.* **2008**, *128*, 194715.
[17] R. Van Lent, S. V. Auras, K. Cao, A. J. Walsh, M. A. Gleeson, L. B. Juurlink, *Science* **2019**, *363*, 155 – 157.
[18] K. Cao, R. van Lent, A. W. Kleyn, M. Kurahashi, L. B. Juurlink, *Proc. Natl. Acad. Sci. USA* **2019**, *116*, 13862 – 13866.
[19] A. C. Luntz, J. K. Brown, M. D. Williams, *J. Chem. Phys.* **1990**, *93*, 5240 – 5246.
[20] B. Poelsema, K. Lenz, G. Comsa, *J. Phys. Condens. Matter* **2010**, *22*, 304006.
[21] K. Cao, R. van Lent, A. W. Kleyn, L. B. Juurlink, *Chem. Phys. Lett.* **2018**, *706*, 680 – 683.
[22] J. E. Ortega, G. Vasseur, I. Piquero-Zulaica, S. Matencio, M. A. Valbuena, J. E. Rault, F. Schiller, M. Corso, A. Mugarza, J. Lobo-Checa, *New J. Phys.* **2018**, *20*, 073010.
[23] T. Michely, G. Comsa, *Surf. Sci.* **1991**, *256*, 217 – 226.
[24] I. M. N. Groot, A. W. Kleyn, L. B. F. Juurlink, *J. Phys. Chem. C* **2013**, *117*, 9266 – 9274.
[25] I. M. N. Groot, A. W. Kleyn, L. B. F. Juurlink, *Angew. Chem. Int. Ed.* **2011**, *50*, 5174 – 5177; *Angew. Chem.* **2011**, *123*, 5280 – 5283.
[26] A. T. Gee, B. E. Hayden, C. Mormiche, T. S. Nunney, *J. Chem. Phys.* **2000**, *112*, 7660 – 7668.
[27] K. Honkala, A. Hellman, I. N. Remediakis, A. Logadottir, A. Carlsson, S. Dahl, C. H. Christensen, J. K. Nørskov, *Science* **2005**, *307*, 555 – 558.

Manuskript erhalten: 22. April 2020
Veränderte Fassung erhalten: 17. Juli 2020
Akzeptierte Fassung online: 4. August 2020
Endgültige Fassung online: 7. September 2020

